

**Journal of
Mechanics of
Materials and Structures**

STRESS SMOOTHING HOLES IN PLANAR ELASTIC DOMAINS

Shmuel Vigdergauz

Volume 5, No. 6

June 2010

STRESS SMOOTHING HOLES IN PLANAR ELASTIC DOMAINS

SHMUEL VIGDERGAUZ

The actual elastostatic problem of optimizing the stress state in a two-dimensional perforated domain by proper shaping of holes is considered with respect to minimization of the global variations of the boundary hoop stresses. This new criterion radically extends the rather restrictive equistress principle introduced by Cherepanov and results in a favorable response of the structure to an external load, with neither local stress concentrations nor underloading of other parts of the boundary. Mathematically, the variations provide an integral-type assessment of the local stresses which requires less computational effort than direct minimization of the stress concentration factor. The proposed criterion can thus be easily incorporated in the numerical optimization scheme previously developed by the author in the closely related context of energy optimization. It includes an efficient complex-valued direct solver and a standard evolutionary optimization algorithm enhanced with an economical shape parametrization tool. The effectiveness of the proposed scheme is illustrated through numerical simulations.

1. Introduction and motivation

Thin and flat construction elements with holes enjoy frequent application in engineering. The holes may cause significant stress concentration and crack initiation, which occur when the resultant maximum hoop stresses σ_h along the hole boundaries L exceeds the material-specific constant σ_0 :

$$\mathcal{H}(L) \equiv \max |\sigma_h(t)| > \sigma_0, \quad t \in L. \quad (1-1)$$

This weakening effect of the holes can be efficiently reduced by their proper shaping to achieve a more favorable stress state of the construction under the same given loading. Such an approach is all the more promising as the hole area usually matters much more than its shape, which thus permits a certain design freedom.

With (1-1), the commonly used criterion for assessing the elastic structure optimality is the minimum of $\mathcal{H}(L)$ over the pool $\{L\}$ of all admissible shapes L_j of each hole:

$$\max |\sigma_h(t)| \equiv \mathcal{H} \xrightarrow{\{L\}} \min; \quad t \in L; \quad L = \bigcup_{j=0}^N L_j. \quad (1-2)$$

The stress-minimizing holes (1-2) maximize the undamaging level of the acting load. The direct problem of evaluating the factor \mathcal{H} over given holes and the inverse problem of its possible minimization are

Keywords: plane elasticity problem, Kolosov–Muskhelishvili potentials, shape optimization, hoop stresses, extremal elastic structures, genetic algorithm.

Preliminary results in this paper were presented at the Fourth European Conference on Computational Mechanics (ECCM 2010), Paris, May 16–21, 2010.

amongst the main topics in elasticity. The related literature is abundant. In the next sections, some relevant papers are commented on for comparison purposes.

Much less attention, however, has been paid to another criterion, according to which the hoop stresses should have *minimal possible variation* along the holes:

$$V[\sigma_h(L)] \xrightarrow{\{L\}} \min. \tag{1-3}$$

In accordance with the general theory of real-valued functions [Natanson 1955], the variation of the stress function is defined as

$$V[\sigma_h(L)] = \sup \sum_j \sum_{i=0}^n |\sigma_h(t_{i+1}^{(j)}) - \sigma_h(t_i^{(j)})|, \tag{1-4}$$

where the supremum is taken over all possible partitions of L_j with an arbitrary system of points $t_0^{(j)}, t_1^{(j)}, \dots, t_n^{(j)}$ ordered by a chosen direction of traversing. For a closed contour we require $t_n^{(j)} = t_0^{(j)}$. Since the variation is always nonnegative and reaches its zero global minimum only at constant-valued functions, i.e.,

$$V[\sigma_h(L)] = 0 \iff \sigma_h(L_j) = C_j \quad \forall j, \tag{1-5}$$

this is an integral measure of how the function is everywhere close to uniformity.

When the constants $\{C_j\}$ are reasonably small, the uniform stress distribution (1-5) presents an ideal response of the structure to an applied external load while avoiding both excessive local stress concentration and underloading of other parts of the boundary at an acceptable stress level.

Though the criteria (1-2) and (1-3) for $V[\sigma_h(L)] > 0$ are implicitly connected through the evident inequality

$$\max \sigma_h(L) - \min \sigma_h(L) \leq V[\sigma_h(L)], \tag{1-6}$$

where the equality sign is attained at, for instance, *any* monotone function, it remains unclear whether they go to their minima together or at each other's expense.

The absolutely nontrivial and purely analytical example here consists of the equistress shapes (ESS) [Cherepanov 1974; Vigdergauz 1976; Banichuk 1977] along which the hoop stresses are simultaneously uniform [Cherepanov 1974] and globally minimal [Vigdergauz 1976]. In other words, an ESS is optimal with respect to *both* criteria, which, for brevity, will be referred to as \mathcal{H} and V , respectively.

However, these shapes exist only under the following restrictive conditions:

- (A₁) The elastic domain is infinite.
- (A₂) The absolute value of the ratio of deviatoric stresses to dilatational stresses externally applied at infinity must be no greater than 1 or, equivalently, the principal remote stresses must have the same sign. Under this requirement, the resultant stress field in the domain remains rather isotropic, thus preserving the ellipticity of the optimization problem.
- (A₃) All the contours must be optimized simultaneously: no fixed holes are allowed.

If all this takes place, the constants C_j are all equal, and are determined only by an external load independently of the number of holes and their relative arrangement. They are found analytically in parallel with the parametric representation of the ESS by solving the Dirichlet problem in a plane with rectilinear slits. See [Milton 2002] and references therein.

Whenever any of the conditions (A₁)–(A₃) is violated, an ESS most likely no longer exists.

A less restrictive *piecewise* constant distribution of the hoop stresses (M -equistressness) was proposed in [Vigdergauz and Cherkaev 1986] and more comprehensively in [Vigdergauz 2006], as an immediate extension of (1-5) to *any* loading at infinity. The M -equistress single hole under remote shear is semi-analytically identified in [Vigdergauz 2006]; two closely spaced holes are numerically found in [Waldman et al. 2003]. Physically, they contain four angular points t_1, \dots, t_4 across which the hoop stresses change sign:

$$\sigma_h(t) = \begin{cases} C', & t_1 < t < t_2, \quad t_3 < t < t_4, \\ C'', & t_4 < t < t_1, \quad t_2 < t < t_3, \end{cases} \quad C', C'' \neq 0, \quad C' C'' < 0, \quad (1-7)$$

so that $V[\sigma_h(L)] = 2|C' - C''|$.

Less constrained optimal problems of this kind have received little or no attention in the literature. We study them here using only the V -criterion, with no additional prerequisites like, say, the piecewise constancy (1-7) of σ_h . The numerical results obtained (Section 5) show that this approach, among other things, reliably reproduces equi- and M -equistressness. In this connection, we note that, as mentioned above, any nonzero variation corresponds to at least an immense variety of monotone functions with the same extrema; thus, the fact that the V -criterion identifies just the independently found piecewise constant M -distributions (when they exist) strongly counts in its favor.

On the other hand, the equistressness (1-5) for a general geometry and the M -equistressness (1-7) for a single hole were first derived as a stationary point of the variation of the strain energy integral over the solid phase with moving boundaries [Cherepanov 1974]. In contrast, we formulate the V -criterion as an essential relaxation of equistressness rather than variationally. Nevertheless, the fact that the stress variation is bounded from below by zero allows one to formulate the V -related shaping of the holes as a global optimization problem (Section 3). A possible relation between energy minimization and the V -criterion deserves a separate study, which is currently beyond our scope.

In the general unrestricted case, the ESS serve as an absolute benchmark to measure the effectiveness of a shape optimization which may be performed now only *separately* for the concentration factor (1-2) and for the variation of the stresses (1-3).

Though both criteria have comparable practical implications, they generalize the ESS in diverging directions. More importantly in the current context, they substantially differ in computational complexity. Indeed, a typical numerical optimization strategy involves two main ingredients: the solution of a given direct problem which has to be repeated many times, and a minimization scheme. The direct solver assesses the fitness of each candidate for optimization by a chosen criterion. The stress concentration factor (1-2), due to its local nature, must be evaluated here with high accuracy to avoid spurious oscillations around the true value, which frequently occur in numerical stress analysis. By contrast, the integral-type criterion (1-3) may be assessed less accurately because the sums (1-4) permit, at least partially, the compensation of numerical errors in the stress computation. The results displayed in Section 5 illustrate that minimization of the variation of the stresses effectively smooths them also outside of limitations (A₁)–(A₃). It works as an oscillation filter within the numerical optimization scheme composed here as follows:

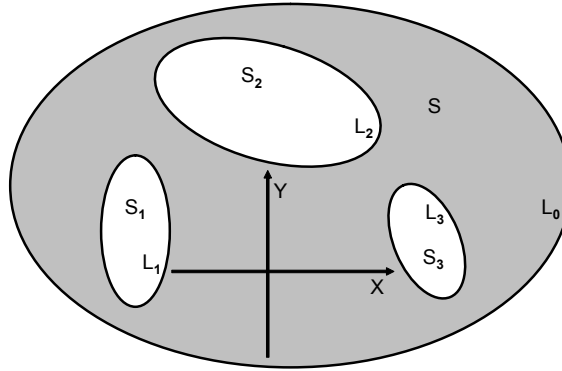


Figure 1. The problem schematic: a two-dimensional elastic region with holes. The outer boundary L_0 may recede to infinity.

- The *direct solver* employs complex-valued Kolosov–Muskhelishvili (KM) potentials [Muskhelishvili 1963], which result in a specially derived system of linear algebraic equations involving no singularities and, hence, providing a fast and accurate assessment of any admissible hole shape.
- The *minimization process* is based on a standardized configured genetic algorithm (GA) which includes the above-described solver for fitness evaluation in a gradientless search of the global optimum. Of importance here is the novel encoding scheme, where each optimized shape is presented *separately* by a sequence of the first N Laurent coefficients of the function mapping it conformally onto a unit circle. As a whole, the proposed scheme was validated previously [Vigdergauz 2008; 2010] in the closely related context of the minimization of the strain energy.

Our contribution, therefore, is twofold: the relaxation of the equistress principle and its efficient numerical implementation.

The paper is organized as follows. In Section 2, the two-dimensional boundary value elastostatic problem for a multiply connected region and the hoop stresses variations is formulated in complex-variable terms. On this basis, Section 3 poses the optimization problem and illustrates its peculiarities by the example of the equistress and the M -equistress shapes. Section 4 described the components of the numerical optimization scheme and how they are combined together. In Section 5, numerical results for a selection of benchmark problems are detailed and discussed to illustrate the validity of our approach and its limitations. Finally, some concluding remarks are made in Section 6.

2. Problem setup and governing equations

Consider, in the complex plane $E : z = x + iy \in E$, a linearly elastic, homogeneous, and isotropic solid S which contains a finite number N of nonintersecting holes S_j with boundaries L_j , $j = 1, \dots, N$, as shown in Figure 1. The infinite region outside the outer boundary L_0 is denoted by S_0 , so $S + \bigcup_{j=0}^N S_j = E$. Each curve L_j , $j = 0, \dots, N$, is supposed to be closed and piecewise smooth, with area F_j . When it exists, the outer boundary L_0 is subject to given external stresses

$$\sigma_{nn}(t) \text{ and } \sigma_{nt}(t), \quad t \in L_0, \quad (2-1)$$

in a local system of curvilinear orthogonal coordinates (n, τ) , while the boundaries of the holes are taken to be traction-free:

$$\sigma_{nn}(t) \equiv 0, \quad \sigma_{n\tau}(t) \equiv 0, \quad t \in L_j, \quad j = 1, \dots, N. \quad (2-2)$$

The load-induced stress tensor $\{\sigma(z)\}$ at any point of the elastic domain is expressed by the complex-valued Kolosov–Muskhelishvili (KM) functions $\Phi(z)$, $\Psi(z)$ holomorphic in S (see [Muskhelishvili 1963] for these and other formulas in this section):

$$\sigma_{xx}(z) + \sigma_{yy}(z) = 4 \operatorname{Re} \Phi(z), \quad z \in S, \quad (2-3a)$$

$$\sigma_{yy}(z) - \sigma_{xx}(z) + 2i\sigma_{xy}(z) = 2[\bar{z}\Phi'(z) + \Psi(z)]. \quad (2-3b)$$

In conformity with the loading conditions (2-1)–(2-2) the KM potentials are linearly linked along the boundary $L = \bigcup_{j=0}^N L_j$ of the solid S by

$$2 \frac{\partial \bar{t}}{\partial t} \operatorname{Re} \Phi(t) + \bar{t}\Phi'(t) - \sigma_{nn}(t) - i\sigma_{n\tau}(t) = -\Psi(t), \quad t \in L_0; \quad (2-4a)$$

$$2 \frac{\partial \bar{t}}{\partial t} \operatorname{Re} \Phi(t) + \bar{t}\Phi'(t) = -\Psi(t), \quad t \in L_j, \quad j = 1, \dots, N. \quad (2-4b)$$

The second potential $\Psi(z)$ is isolated in the right-hand side of (2-4) for future use (see Section 4.1). When the elastic domain is infinite, the outer boundary L_0 does not exist and the nonzero conditions (2-4a) are replaced by the given far-field principal stresses $\sigma_{xx}^\infty = P$, $\sigma_{yy}^\infty = Q$, $\sigma_{xy}^\infty = 0$, which dictate the asymptotics

$$\Phi(z) = Bz + O(|z|^{-2}), \quad 4B = P + Q, \quad z \rightarrow \infty; \quad (2-5a)$$

$$\Psi(z) = \Gamma z + O(|z|^{-2}), \quad 2\Gamma = Q - P. \quad (2-5b)$$

The identities (2-4a)+(2-4b) or (2-4a)+(2-5) form a boundary value problem to be solved for KM potentials, which in turn define the resultant stresses through (2-3). Using the traction-free condition (2-4b) and the coordinate invariance of the stress tensor trace in the left side of (2-3a) we obtain, along each inner hole,

$$\sigma_{\tau\tau}(t) = 4 \operatorname{Re} \Phi(t), \quad t \in L_j, \quad j = 1, \dots, N, \quad (2-6)$$

and, in like manner, when the outer boundary is present,

$$\sigma_{\tau\tau}(t) = 4 \operatorname{Re} \Phi(t) - \sigma_{nn}(t), \quad t \in L_0. \quad (2-7)$$

Here $\sigma_{\tau\tau}(t)$ denotes the hoop stresses abstractly written in Section 1 as σ_h . In view of (2-6), (2-7), their total variation is written as

$$V[\sigma_{\tau\tau}(L)] = \sum_{j=0}^N V[\sigma_{\tau\tau}(L_j)] = 4 \sum_{j=0}^N V[\operatorname{Re} \Phi(L_j) - \delta_{j,0}\sigma_{nn}(L_j)] \quad (2-8)$$

where $\delta_{j,0}$ stands for the Kronecker delta.

At a fixed external load, the stresses and hence their boundary variations depend only on a number of the holes, their shape, size and mutual arrangement. As it will be shown later, the hole shapes admit an effective finite parametrization, which significantly facilitates the numerical shape optimization technique with respect to the V -criterion.

3. Problem formulation

We are now in a position to define more precisely the problem (1-3) of minimizing the variation of the hoop elastic stresses in complex-variable terms:

Given relative locations and areas of a number of traction-free holes in a two-dimensional thin elastic domain, find the hole shapes L_j that minimize the hoop stresses variation (1-3)+(2-8) under a load specified either along a fixed outer boundary by (2-1)+(2-4a) or at infinity by (2-5).

Except for the novel criterion, this is a standard shape optimization problem in elasticity.

As already noted, the global minimum (1-5) of the variation criterion V is reached, for instance, at the equistress holes in an infinite plate; they are derived in the current terms as follows.

Substitution of (1-5) into (2-6) gives at the inner traction-free holes

$$\operatorname{Re} \Phi(t) = C_j, \quad j = 1, \dots, N. \quad (3-1)$$

The identities (3-1) and the bulk-type asymptotics (2-5a) form the elementary Dirichlet problem in the holomorphic function $\Phi(z)$ with the unique solution

$$\Phi(z) = \text{constant} = B, \quad z \in S; \quad C_j = B, \quad j = 1, \dots, N; \quad (3-2)$$

which is valid for *any* hole shapes and locations. By (3-2), the traction-free condition (2-4a) then simplifies to the boundary-value problem in the second KM potential $\Psi(z)$

$$\Psi(t) = -2B \frac{\partial \bar{t}}{\partial t}, \quad t \in L_j, \quad j = 1, \dots, N, \quad (3-3)$$

with shear-type asymptotics (2-5b) at infinity. In contrast to (3-1), this problem may have a solution only for *specifically shaped* holes along which the right-hand side of (3-3) is the boundary value of a function holomorphic in S . The bulk-type asymptotics (2-5) provides a necessary condition for solvability of the problem. Indeed, taking the absolute values of both sides of (3-3) and using the evident fact that

$$\left| \frac{\partial \bar{t}}{\partial t} \right| \equiv 1, \quad t \in L, \quad (3-4)$$

for any arc L in the complex plane, we have

$$|\Psi(t)| = 2 \left| B \frac{\partial \bar{t}}{\partial t} \right| = 2|B|. \quad (3-5)$$

Since the modulus of a holomorphic function is a real subharmonic function of z [Courant 1950], it obeys the maximum principle and hence achieves its maximum only at the domain boundary L . Particularly

$$|\Psi(z = \infty)| = |\Gamma| \leq 2|B| \quad (3-6)$$

or, in equivalent form, $\Delta \equiv \Gamma/(2B)$, which implies

$$|\Delta| = \left| \frac{\sigma_{yy}^\infty - \sigma_{xx}^\infty}{\sigma_{yy}^\infty + \sigma_{xx}^\infty} \right| \leq 1, \quad (3-7)$$

a quantitative expression of the solvability condition (A₂) discussed in Section 1.

In themselves, the equistress shapes are found parametrically by the conformal mapping of the optimized infinite domain into a plane with parallel slits [Cherepanov 1974] where the transformed boundary conditions (3-3) are met. For further references, we reproduce here the equations for the upper side of the right hole in the case of two identical ESS disposed symmetrically about the y -axis [Cherepanov 1974]:

$$\left. \begin{aligned} \frac{y(\xi)}{C} &= (1 + \gamma) \left(E(\theta, \sqrt{1 - \xi_0^2}) + d_0 F(\theta, \sqrt{1 - \xi_0^2}) - R(\xi) \right) \\ \frac{x(\xi)}{C} &= x_0 + (1 - \gamma)(\xi - \xi_0) \end{aligned} \right\} \text{ for } 0 < \xi_0 \leq \xi \leq 1, \quad (3-8)$$

where

$$\begin{aligned} \theta &= \arcsin \frac{1}{\xi} \sqrt{\frac{\xi^2 - \xi_0^2}{1 - \xi_0^2}}, & x_0 &= (1 - \gamma)\xi_0 + (1 + \gamma) \left(E\left(\frac{\pi}{2}, \xi_0\right) - (1 + d_0)F\left(\frac{\pi}{2}, \xi_0\right) \right), \\ d_0 &= -\frac{E\left(\frac{\pi}{2}, \sqrt{1 - \xi_0^2}\right)}{F\left(\frac{\pi}{2}, \sqrt{1 - \xi_0^2}\right)}, & R(\xi) &= \xi^{-1} \sqrt{(1 - \xi^2)(\xi^2 - \xi_0^2)}. \end{aligned}$$

Here F and E are the elliptic integrals of the first and second kind, respectively, C denotes a nonessential scaling factor up to which the two-hole geometry is described by the single dimensionless parameter λ , the ratio of the half interdistance x_0 to the square rooted area $F_1 = F_2$ of either of the holes:

$$\lambda = \frac{x_0}{\sqrt{F_{1,2}}}, \quad 0 < \lambda < \infty. \quad (3-9)$$

With decreasing distance x_0 , and, hence, increasing interaction between the holes, the resultant optimal shape (3-8) evolves from an ellipse to a kidney-like shape, as illustrated in [Cherepanov 1974].

The seeming ease of obtaining the globally optimal solution (3-8) is completely due to the conditions (A₁)–(A₃) listed in Section 1, which make it possible to preliminary find the first KM potential $\Phi(z)$ in the geometry-independent form (3-2). Other examples of the ESS such as a circular hole under uniform pressure are too trivial to be considered.

Now it becomes clear how the loading inequality (3-6) works. Indeed, consider a single traction-free hole under remote shear [Vigdergauz and Cherkvaev 1986]: then $B = 0$ and $\Gamma = 1$. The nonzero equistress condition (3-1) then makes no sense in view of the mean value theorem for a harmonic function $\text{Re } \Phi(z)$ [Courant 1950], by which

$$\widehat{\text{Re } \Phi}(t) = C_1 = \text{Re } \Phi(\infty) = B \equiv 0, \quad t \in L_1, \quad (3-10)$$

where the hat denotes the function’s mean value along L_1 . In contrast, the weakened M -equistress condition (1-7) is compatible with (3-10) provided that $C' = -C''$ and $\arg t_k = (2k - 1)i\pi/4$ ($k = 1, 2, 3, 4$), as dictated by the problem’s rotational symmetry. Again, as above, substitution of (1-7) into the boundary condition (2-4a) and conformal mapping help to find the shape and the stress constant C' [Vigdergauz and Cherkvaev 1986], this time only numerically. The optimal shape looks like a slightly rounded square. A more efficient semianalytical approach [Vigdergauz 2006] is given in Section 5 for comparison.

The general case, however, does not lend itself to solution by this approach and the whole situation calls for a numerical treatment based on a novel analytical approach.

4. Numerical scheme

Particularly relevant to the present purposes, is the scheme previously developed in [Vigdergauz 2008; 2010], in the similar context of the energy-related shape optimization. For completeness and reader’s convenience, its basic features are briefly outlined below.

4.1. Direct solver. It is shown in the previous section that the ESS allow one to find the KM potentials (a) sequentially rather than in parallel, and (b) in closed form.

Actually, however, $\Phi(z)$, $\Psi(z)$ can be separated for any set of hole shapes, though in a quite different manner and only numerically. As compared to the standard practice, this option halves the computational complexity of the direct problem. Crucial here is that, in contrast to $\Phi(z)$, the second potential $\Psi(z)$ enters the boundary conditions (2-4) with neither conjugates nor derivatives. This offers a way of solving (2-4) as a regular boundary-value problem in only $\Phi(z)$ and, when needed, to find $\Psi(z)$ by simple integration thereafter.

Indeed, since the Cauchy-type integral of the holomorphic function $\Psi(z)$, $z \in S$, over L vanishes identically in each complementary region S_j , $j = 0, \dots, N$ [Ahlfors 1978], we have from (2-4)

$$\int_L \frac{2 \operatorname{Re} \Phi(t) d\bar{t} + \bar{t} \Phi'(t) dt}{t - z} = \int_{L_0} \frac{\sigma_{nn}(t) + i \sigma_{n\tau}(t)}{t - z} dt, \quad \forall z \in S_j, \quad j = 0, \dots, n. \tag{4-1}$$

Here L is traversed in the positive direction with respect to the elastic domain S .

Evidently, a Taylor-like expansion of the Cauchy kernel $1/(t - z)$ around arbitrary finite points $a_j \in S_j$, $j = 1, \dots, n$, namely

$$\frac{1}{t - z} = \frac{1}{t - a_j} + \sum_{k=1}^{\infty} \frac{(z - a_j)^k}{(t - a_j)^{k+1}}, \quad |z - a_j| < \epsilon, \quad j = 1, \dots, N, \tag{4-2}$$

is absolutely convergent at least for a sufficiently small ϵ . Similarly, at infinity,

$$\frac{1}{t - z} = -\frac{1}{z} - \sum_{k=1}^{\infty} \frac{t^k}{z^{k+1}}, \quad |z| > R, \tag{4-3}$$

for a sufficiently large R .

Next, substitution of (4-2) and (4-3) into (4-1) and equating like powers on both side yields the infinite set of identities ($k = 1, 2, \dots$)

$$\int_L \frac{2 \operatorname{Re} \Phi(t) d\bar{t} + \bar{t} \Phi'(t) dt}{(t - a_j)^k} = \int_{L_0} \frac{\sigma_{nn}(t) + i \sigma_{n\tau}(t)}{(t - a_j)^k} dt; \quad j = 1, \dots, N, \tag{4-4a}$$

$$\int_L (2 \operatorname{Re} \Phi(t) d\bar{t} + \bar{t} \Phi'(t)) t^{k-1} dt = \int_{L_0} (\sigma_{nn}(t) + i \sigma_{n\tau}(t)) t^{k-1} dt. \tag{4-4b}$$

By the principle of analytical continuation [Ahlfors 1978], these identities are valid not only near the points $\{a_j\}$ but everywhere outside S . Therefore, taken together, they are equivalent to the initial boundary conditions (2-4). Finally, the Laurent series of $\Phi(z)$ around the same points a_j and at infinity,

$$\Phi(z) = \sum_{j=1}^n \sum_{k=2}^{\infty} \frac{d_j^{(k)}}{(z - a_j)^k} + \sum_{k=2}^{\infty} \frac{d_0^{(k)}}{z^k}, \quad z \in S, \tag{4-5}$$

transforms (4-4) into an infinite set of linear algebraic equations

$$A\vec{x} = D, \quad A = \{A_{kl}\}, \quad D = \{D_k\}, \quad (4-6)$$

for the unknowns $\vec{x} = \{d_j^{(k)}\}$, with $j = 0, \dots, N$ and $k = 2, \dots$. The coefficients of the system involve *regular* rather than *singular* integrals and hence are computationally more advantageous than the conventional integral equation schemes [Muskhelishvili 1963]. For certain geometries, they are displayed in Section 5. When S is infinite, the integrals along the outer contour L_0 are discarded together with the coefficients $\{d_0^{(k)}\}$, while the right-hand side of the system is a linear combination of specific integrals over all holes with the loading coefficients B and Γ from (2-5) as detailed in [Vigdergauz 2008; 2010]. In both cases, the system involves only the first KM potential $\Phi(z)$ and hence has a halved size when truncated for numerical purposes to a finite number N_{sys} . The number of the unknowns may be further reduced for a problem with symmetry as shown for specific cases in Section 5.

4.2. Shape encoding algorithm. The key issue in numerical applications of the proposed solver is how to effectively parametrize hole shapes, both for evaluating the contour integrals (4-4) in the system coefficients and optimizing the shapes over the same parameters. A workable approach here is a conformal mapping of the domain D outside a unit circle $\rho = \exp i\theta$, $0 \leq \theta \leq 2\pi$, $|\rho| = 1$, onto the infinite domain $E_j \equiv E - S_j$ performed *separately* [Vigdergauz 2008; 2010] for each shape L_j , $j = 0, \dots, N$, by $N+1$ functions with a finite Laurent expansion in D :

$$\frac{\omega_j(\zeta)}{C} = \zeta + \sum_{m=1}^M \frac{b_m^{(j)}}{\zeta^m} \quad \text{with } |\zeta| \geq 1, \quad j = 0, \dots, N, \quad (4-7)$$

where C is the scaling coefficient at which

$$\omega_j(\rho) = t \in L_j, \quad j = 0, \dots, N. \quad (4-8)$$

Taken as design variables, the mapping coefficients $b_m^{(j)}$, with $m = 1, \dots, M$ and $j = 0, \dots, N$, offer a number of substantial advantages over the commonly used nodal point shape representation, as detailed in [Vigdergauz 2010]. First, the conformal mapping-based description (4-8) is *continuous* rather than discrete, and hence even a small number M of them gives a wide variety of smooth closed shapes as compared to tens and hundreds of nodal points required for the same purpose. This is all the more so because the $b_j^{(m)}$ are bounded by the successively narrowed intervals

$$-\frac{1}{\sqrt{m}} \leq b_m^{(j)} \leq \frac{1}{\sqrt{m}}, \quad j = 0, \dots, N, \quad m = 1, 2, \dots \quad (4-9)$$

(see [Ahlfors 1978]), which are the necessary condition for the nonnegativeness of the area F_j inside L_j :

$$F_j = \pi \left(1 - \sum_{m=1}^M m |b_m^{(j)}|^2 \right), \quad j = 0, \dots, N. \quad (4-10)$$

As a result, high-order coefficients are mostly responsible for forming large local curvatures and have little impact on the integral-type criterion (2-8) of minimum stress variation. Second, with the identities

$$\bar{\rho} = \rho^{-1}, \quad d\rho = \rho d\theta, \quad dt = i\omega'_j(\rho)\rho d\theta, \quad d\bar{t} = -i\overline{\omega_j(\rho)}\rho^{-1} d\theta, \quad t \in L_j, \quad (4-11)$$

the integration path L_j is continuously transformed into the unit circumference ρ , thus making the numerical integration easier and independent of the parameter M . In numerical simulation (Section 5) we use the simplest trapezoid rule with N_{int} equal subintervals.

In a multiply connected case, the parametrization (4-7)–(4-11) also does better numerically than the canonical simultaneous mapping [Courant 1950] of an infinite plane ζ with N slits or holes by a holomorphic function $\omega(\zeta)$. Indeed, the boundary condition in ζ [Muskhelishvili 1963]

$$-\frac{2}{\zeta^2} \overline{\omega'(\zeta)} \operatorname{Re} \Phi(\zeta) + \overline{\omega(\zeta)} \Phi'(\zeta) + \omega'(\zeta) \Psi(\zeta) = 0, \quad \zeta \in L, \tag{4-12}$$

is more complicated than its unmapped counterpart (2-4b) and, most likely, may not be simplified beyond the nice exception of the equistressness. Further, the proposed approach easily meets any given arrangement of the holes by displacing the separate maps (4-7) in the physical plane E :

$$\omega_j(z) \rightarrow \omega_j(z) + h_j, \quad j = 1, \dots, N. \tag{4-13}$$

Here the h_j are complex-valued constants. This can hardly be done by an ordinary mapping of the whole domain S as exemplified in Section 3, where the implicit relation in (3-8) between the ESS interdistance x_0 and the auxiliary parameter λ is not invertible analytically to give λ as a function of ξ_0 . This is all the more true for fixed shapes. When they exist, they are necessarily involved into the usual mapping, and should be restored through a nonlinear boundary condition imposed on the holomorphic function $\omega(\zeta)$, while separate mapping simply does not touch them. Finally, we note that the parametrization works well up to closely spaced holes (see Section 5) with a relatively small number M of the Laurent terms in (4-7).

4.3. Fitness evaluation. Once the hoop stresses $\sigma_{\tau\tau}(t)$ are found through $\Phi(z)$, the fitness of the corresponding set of the holes can be next evaluated with respect to the minimum variation criterion (2-8)+(1-4). Of course, for numerical implementation, the supremum in (1-4) is replaced by the sum over only one selection of q closely spaced points $0 = x_1 < x_2 < \dots < x_q = 2\pi$ along each hole contour. We select the points x_p in the form

$$x_p = \pi(1 + \beta_p^{(q)}), \quad p = 1, \dots, q, \tag{4-14}$$

where the $\beta_p^{(q)}$ are the roots of the Chebyshev polynomials of the second kind

$$U_q(x) = \prod_{p=1}^q (x - \beta_p^{(q)}), \quad \beta_p^{(q)} = \arccos \frac{p\pi}{q+1}, \tag{4-15}$$

widely used in approximation theory. In the current context, their especially relevant property stems from the fact that the $U_n(x)$ are known [Abramowitz and Stegun 1964] to minimize the integral

$$\int_{-1}^1 P_q(x) dx \xrightarrow{\{P_q\}} \int_{-1}^1 U_q(x) dx \tag{4-16}$$

among all polynomials $P_q(x)$ of same degree q and same leading coefficient. On the other hand, the variation of a differentiable function $f(x)$ in an interval takes the form [Natanson 1955]

$$V_a^b(f) = \int_a^b |f'(x)| dx, \tag{4-17}$$

in conformity with the general definition (1-4). Comparison of (4-17) with (4-16) shows that $V_{q+1}(x) : V'_{q+1} \equiv U_q(x)$, $q \geq 1$, are the polynomials of the minimum variation in $[-1, 1]$. The numerical simulation (Section 5) indicate that the usage of (4-14) adds some 6 to 8 percent to the accuracy of the results obtained with the same number of uniformly distributed approximation points.

Finally (4-17) gives

$$V_a^b(f) = \int_a^b |f'(x)| dx \geq \left| \int_a^b f'(x) dx \right| = |f(b) - f(a)|, \quad (4-18)$$

where the equality holds if and only if $f'(x)$ has constant sign on $[a, b]$. This means that V -optimization seeks to smooth the stresses distribution by making it monotonous on the irreducible part of the contour. We have already noted that the proposed criterion, in fact, does even more. Amongst monotone distributions it tends to find a piecewise constant one, as exemplified in Section 5.

4.4. Evolutionary optimization scheme. With the mapping terms (4-7), the optimization problem is finally reformulated as follows

$$V[\sigma_{\theta\theta}(L)] \xrightarrow{\{b_m^{(j)}\}} \min(\hat{b}_m^{(j)}, m = 1, \dots, M, j = 0, \dots, N). \quad (4-19)$$

Put another way, the search space for each shape L_j is reduced to a M -dimensional rectangular parallelepiped with edges of length $2/\sqrt{m}$, $m = 1, \dots, M$, as defined by bilateral inequalities (4-9). They form a set of linear constraints on the definition domain of the nonlinear minimized function $V(b_1^{(0)}, \dots, b_M^{(N)})$, thus completing the problem formulation.

Our previous experience [Vigdergauz 2008; 2010] suggests that the computational process of shape optimization (4-19)+(4-9) can be effectively conducted by evolutionary genetic algorithms (GAs), which have been well-accepted in the last two decades (see, for instance, [Goldberg and Sastry 2010] and references therein). They perform a gradientless optimization in a large search space by mimicking the Darwinian process of natural selection over successive generations through crossover and mutation operations. The efficient direct solver and the time-saving shape encoding numerically simplify the parametrized optimization problem (4-19), allowing the use of an ordinary genetic algorithm configuration, as detailed in our papers just cited. A set $\{L\}$ of shapes is stochastically generated into a ‘‘chromosome’’ encoding $M \times (n+1)$ mapping parameters (4-7) as signed 16-bit integers r_j^m , in conformity with (4-9):

$$b_j^{(m)} = \frac{r_j^m}{I\sqrt{m}} \quad \text{with } I = 2^{15} - 1, \quad -I \leq r_j^m \leq I, \quad j = 0, \dots, n, \quad m = 1, 2, \dots \quad (4-20)$$

The proposed direct solver permits evaluating the fitness of the chromosome that is the stresses variation for the decoded shapes $L(b_j^{(m)})$. An initial family of N_{chr} chromosomes is then subject to genetic operations of recombination, crossover and mutation performed over the integers $\{r_j^m\}$ rather than over $\{b_j^{(m)}\}$. In doing so, the best individuals with the minimal fitness have the highest chance of surviving in the offspring which in turn is passed to the fitness evaluation stage, and the cycle continues until the search is terminated. The number N_{iter} of iterations should be taken sufficiently large to ensure close proximity of the solution to the global minimum. As is customary in iterative optimization, we indirectly estimate the proximity by the inner stability of the process when the obtained minimum remains unchanged

through a number of successive evolutionary steps. In general, the efficiency of GAs strongly depends on the parameters involved, which, when chosen poorly, may slow convergence or even result in failure.

Of course, the scheme above described is not the only possible way to solve the shape optimization problem at hand. For instance, [Waldman et al. \[2003\]](#) combine the finite element analysis with the specially designed gradientless scheme of shape optimization by the M -equistress criterion (1-7) when the elastic material is added at regions of high stress and/or removed where the hoop stress is low. In contrast to our approach, this procedure needs an initial guess for the shapes to start with. As a result, a given mutual arrangement of the holes is generally not preserved after optimization. Besides, the authors use a time-consuming remeshing between iterations to avoid mesh distortion. Qualitatively, their results fully agree with ours, though quantitative discrepancies are rather significant for two closely spaced optimal holes in a plane under shear dominating far load. The details are discussed in [Section 5.3](#).

5. Numerical results

As already noted, the evaluation of the variation under the proposed optimization scheme depends on a number of parameters such as the probabilities of the GA operations, the truncated system size N_{sys} , and the numbers N_{int} , M , and q of, respectively, integration points, mapping terms, and Chebyshev polynomial roots. All must be pre-adjusted to obtain stable and reliable solutions. We do it here using a rare opportunity of comparing the numerical results with the corresponding closed solution (3-8) for two equistress holes ([Section 5.1](#)). Further, in order to validate the approach, we numerically simulated a number of yet unsolved two-dimensional cases.

5.1. Two equistress holes in an infinite plate under uniaxial tension ($B = 1, \Gamma = 0$). Here our aim is to identify the ESS numerically with the minimum variation criterion (2-8) instead of using the equistress principle (3-1)+(3-2) as a prerequisite.

Let two identical holes be located symmetrically with respect to the Cartesian axes. Then $\Phi(z)$ is even and takes conjugate values at complex conjugate points [[Muskhelishvili 1963](#)]:

$$\Phi(z) = \Phi(-z), \quad \Phi(\bar{z}) = \overline{\Phi(z)}, \quad z \in S + L \tag{5-1}$$

With this in view, the Laurent expansion (4-5) simplifies to

$$\Phi(z) = \sum_{k=2}^{\infty} d_k^{(1)} \left(\frac{1}{(z - a_1)^k} + \frac{(-1)^k}{(z + a_1)^k} \right), \quad z \in S + L, \quad a_1 \in S_1; \quad \text{Im } d_k^{(1)}, \quad k = 2, 3, \dots, \tag{5-2}$$

and the system (4-6) takes the form

$$A_{kl} = 2l \int_{L_1} \text{Re}(\rho_{l+1}(t, c)) \rho_k(t, c) d\bar{t} + l(l+1) \int_{L_1} \bar{t} \rho_{l+2}(t, c) \rho_k(t, c) dt, \tag{5-3a}$$

$$D_k = -4B \int_{L_1} \rho_k(t, c) d\bar{t}, \quad k = 0, 1, 2, \tag{5-3b}$$

$$\rho_0(t, z) \equiv \frac{1}{t-z} + \frac{1}{t+z}, \quad z \in S_1, \tag{5-3c}$$

$$\rho_k(t, c) \equiv \frac{1}{k!} \frac{\partial^k \rho_0(t, z)}{\partial z^k} \Big|_{z=a_1} = \frac{1}{(t - a_1)^{k+1}} + \frac{(-1)^k}{(t + a_1)^{k+1}}, \tag{5-3d}$$

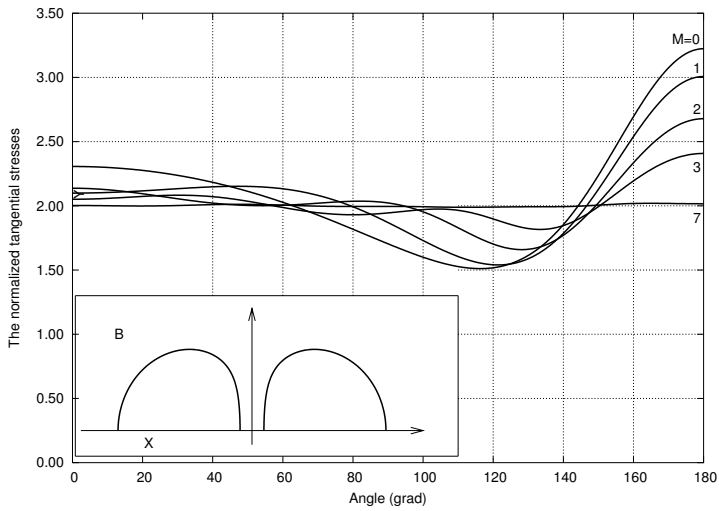


Figure 2. Two holes under remote bulk loading: the V -optimal hoop stresses $\sigma_{\tau\tau}(\theta)$ as a function of the mapping size M at $\lambda = 0.2$.

Finally, when replacing $t \in L_1$ by its map (4-7)+(4-8), we define the scaling factor C and the displacement (4-13) (separately for each generated shape) to keep a given geometrical parameter λ from (3-9). By virtue of symmetry, the mapping terms $b_m^{(1)}$, $m = 1, \dots, M$ are also real and the integration in (5-3) is performed only along the upper half of $L_1 : 0 \leq \theta \leq \pi$.

Figure 2 depicts the convergence of the resultant hoop stresses on the optimized contour L_1 to the uniform distribution (3-2) at $\lambda = 0.2$ in dependence on the mapping problem size M , beginning with a circle $M = 0$. As one would expect, the largest local deviation of the hoop stresses is observed near the point x_0 , ($\theta = \pi$) closest to the opposite hole. Figure 3 shows the optimally smoothed stresses at $M = 9$

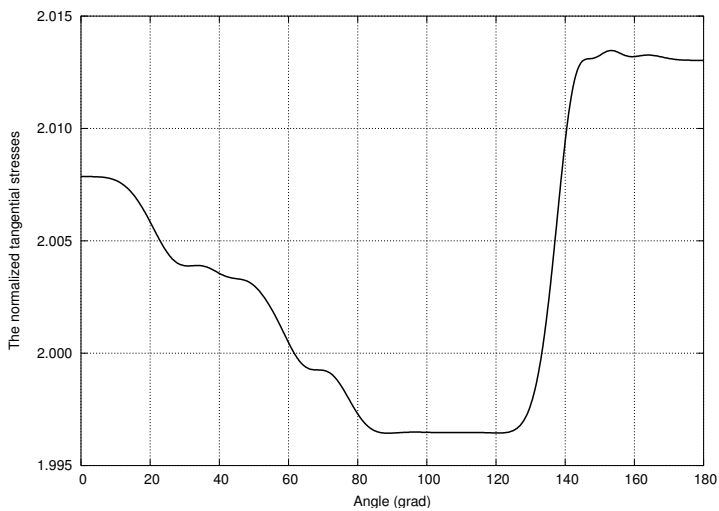


Figure 3. Two holes under remote bulk loading: the V -optimal hoop stresses for $M = 9$ in an enlarged scale.

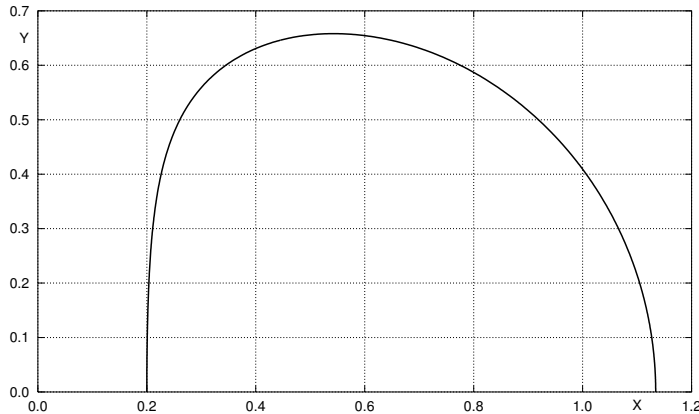


Figure 4. Two holes under remote bulk loading: the upper half of the right V -optimal hole at $\lambda = 0.2$.

in an enlarged scale. The maximum relative error of $\sigma_{\theta\theta}$ is approximately 0.65%. We believe that the error can be further reduced at the expense of increasing the computational cost but it is not our current aim. Figure 4 depicts the numerically obtained optimal shape which is compared with the parametric equations (3-8) taken at the computed value $\xi_0 \approx 0.0024051725$, $\lambda(\xi_0) = 0.2$. The mutual deviations are too small to be seen here. This closeness provides empirical grounds for adjusting the parameters listed at the beginning of the section. Table 1 gives their calibrated values used in further calculations.

GA parameter	Parameter value(s)
Gene	Integer in $[-32767; 32767]$
Individual	Interface shape
Population size	800
Number of genes, M	up to 9
Initial population	800 random individuals
Selection	Tournament
Elitism	Four best individuals
Crossover	1-point
Crossover rate	0.90
Creep mutation	By randomly changing a bit
Creep mutation rate	0.35
Jump mutation	By adding a random integer, typically in the range $[-4; 4]$
Jump mutation rate	0.35
Stopping criterion	After 1200 iterations
Resolving system size K	36
Number of integration points N_p	720 (in the interval $[0, \pi]$)
Number q of sample points on contour	1440

Table 1. GA operator types, their probability rates and related parameters typically used in further optimizations.

5.2. A single V -optimal hole in infinite plate under remote shear ($\mathbf{B} = \mathbf{0}$, $\mathbf{\Gamma} = \mathbf{1}$). Here, the rotational properties of the problem imply that $\Phi(iz) = -\Phi(z)$ and hence

$$\Phi(z) = \sum_{k=1}^{\infty} \frac{a_{4k-2}^{(1)}}{z^{4k-2}}; \quad \frac{\omega_1(\zeta)}{C} = \zeta + \sum_{m=1}^M \frac{b_{4m-1}^{(1)}}{\zeta^{4m-1}}, \quad |\zeta| \geq 1, \tag{5-4}$$

while the right-hand side of the system (4-6) takes the form

$$D_0 = -2\Gamma_0, \quad D_k = 0, \quad k = 1, 2, \dots \tag{5-5}$$

In conformity with (3-10) and (5-4) we have

$$\sigma_{\theta\theta}(e^{i\pi/2}\zeta) = -\sigma_{\theta\theta}(\zeta), \quad \widehat{\sigma_{\theta\theta}(\zeta)} = 0. \tag{5-6}$$

Remarkably, for a single hole an M -term finite mapping expansion generates *exactly* a finite $M \times M$ system [Vigdergauz 2006]. This allows one to avoid additional truncation error by explicitly summing the infinite tail of the series (5-4) through a finite difference scheme. As a result, the hoop stresses along any hole are obtained as rational functions of the nonzero mapping terms $b_{4m-1}^{(1)}$, $m = 1, \dots, M$. In particular, for $M = 1$ we have [Vigdergauz 2006]

$$\sigma_{\theta\theta}(\xi) = \frac{4(1 - 3b_3) \cos 2\theta}{(1 - b_3)(1 - 6b_3 \cos 4\theta + 9b_3^2)}, \quad b_3 = b_3^{(1)}. \tag{5-7}$$

This makes the fitness evaluation equally easy and accurate for any criterion of optimality. Table 2 compares the computed V - and \mathcal{H} -optima and the corresponding mapping terms for various M . The \mathcal{H} -related values, in parentheses, are taken from [Vigdergauz 2006]. It is seen that with increasing M , both sets come closer and closer together; this is further illustrated in Figure 5. The V - and \mathcal{H} -optimal stress

N	$b_3^{(1)}$	$b_7^{(1)}$	$b_{11}^{(1)}$	$b_{15}^{(1)}$	$b_{19}^{(1)}$	$b_{23}^{(1)}$	V_{\min}	\mathcal{H}_{\min}
3	-0.07110 (-0.09000)						3.15744	3.11765 (3.07165)
7	-0.09681 (-0.11162)	0.00444 (0.00751)					2.96826	2.95683 (2.90563)
11	-0.10987 (-0.12182)	0.00733 (0.01044)	-0.00090 (-0.00200)				2.88768	2.88003 (2.84110)
15	-0.11748 (-0.12732)	0.00918 (0.01210)	-0.00165 (-0.00293)	0.00027 (0.00076)			2.84435	2.84159 (2.80824)
19	-0.12991 (-0.13049)	0.01055 (0.01293)	-0.00221 (-0.00340)	0.00055 (0.00112)	-0.00011 (-0.00032)		2.81818	2.81517 (2.78843)
23	-0.12498 (-0.13059)	0.01093 (0.01292)	-0.00239 (-0.00338)	0.00064 (0.00116)	-0.00017 (-0.00041)	0.00003 (0.00010)	2.80387	2.80262 (2.77936)

Table 2. A single square symmetric hole under remote shear: conformal mapping coefficients and the V -criterion resulting from the GA optimization process for different values of N . The \mathcal{H} -related values are also shown for comparison, in parentheses.

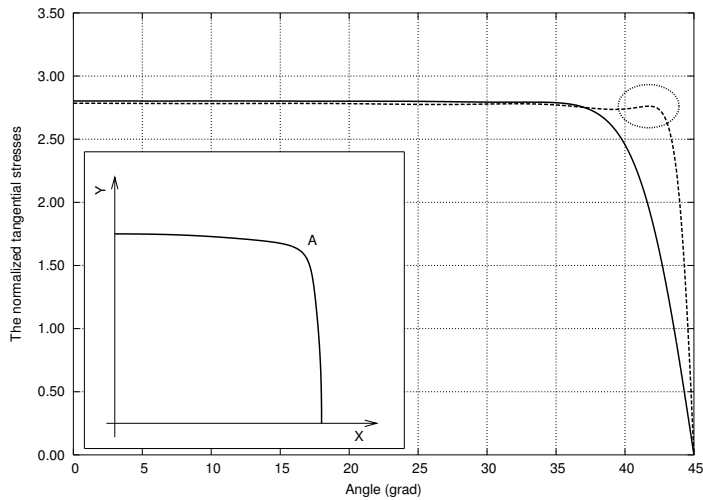


Figure 5. A single square symmetric hole under remote shear: tangential stress distribution along the V - and \mathcal{H} -optimal holes (solid and dashed lines, respectively) for $M = 23$. The local nonmonotonicity of the \mathcal{H} -related curve is marked with an ellipse.

distributions at $M = 23$ are very similar except for a vicinity of the angular point ($\theta = \pi/4$) where the criteria work differently. As explained at the end of Section 4.3, the V -optimal stress distribution tends to be monotonous while the \mathcal{H} -criterion further diminishes the stress maximum with some sacrifice in monotonicity. In any case, the difference between two maxima is hardly greater than the computational errors. This favors in the V -criterion ability. We may conservatively conclude that again, as in the equistress case, the \mathcal{H} - and V -optimal single holes under pure shear are very similar to each other, if not the same. Figure 6 depicts the evolution of the V -optimal shape with increasing M . One clearly sees the smooth formation of an angular point with higher mapping coefficients.

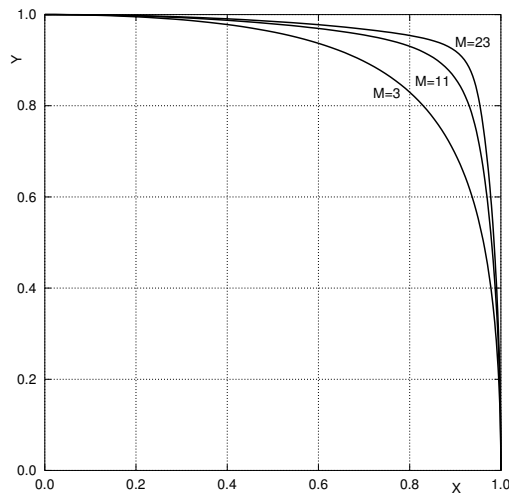


Figure 6. A single square symmetric hole under remote shear: the M -related evolution of the V -optimal hole.

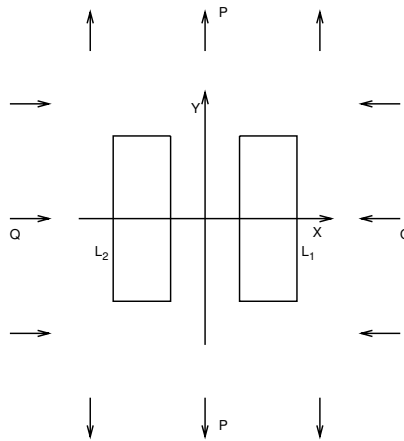


Figure 7. An infinite plate with two identical holes under pure shear. The hole shapes are symmetric about the x -axis and may have a finite number of angular points.

5.3. Two V -optimal holes in an infinite plate under remote shear ($B = 0$, $\Gamma = 1$). The corresponding setup is shown in Figure 7. The only computational difference from the equistress case (Section 5.1) is in the right-hand side (5-3b) of the resolving system (5-3). Now it has the form (5-5) [Vigdergauz 2008].

It is worth noting the following. Our previous experience [Vigdergauz 2008; 2010] shows that, by contrast to (5-3b), the shear-type loading vector (5-5) results in low stability and accuracy of computing the local stresses which are polluted with spurious oscillations. The reason is that the shear-type optimal problem is no more elliptic as (3-2), and hence its solution loses some regular properties. For a single hole (Section 5.2) it was compensated by an analytical summation of the infinite series in (5-4). Here, as before, the numerically implemented V -criterion works equally well. Figure 8 illustrates this

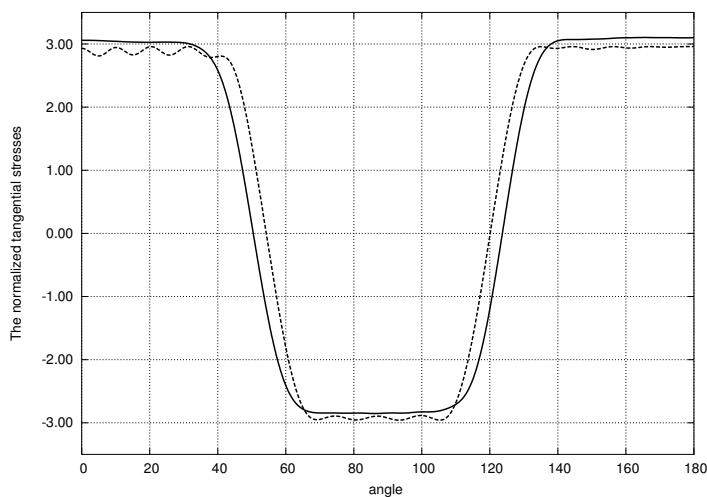


Figure 8. An infinite plate with two identical holes under pure shear: the V - and \mathcal{H} -optimal stresses (the dashed line) obtained by the same numerical scheme at $\lambda = 0.2$ are compared to demonstrate the distinctive V -related smoothing effect.

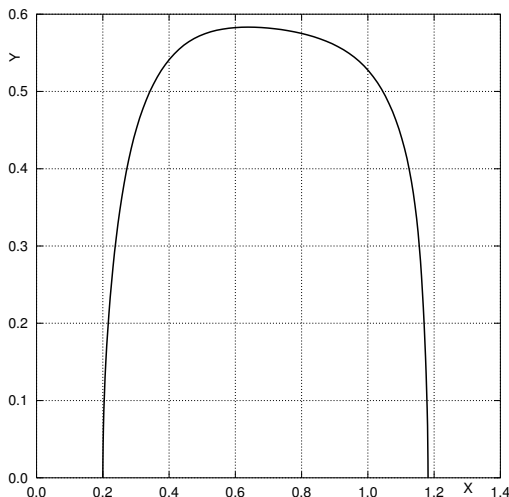


Figure 9. An infinite plate with two identical holes under pure shear: the upper half of the right V -optimal hole at $\lambda = 0.2$.

conclusion, exemplifying the V -related filtering effect for two closely spaced holes at $\lambda = 0.2$ whose shape is given in Figure 9. In contrast to the square symmetric V -optimal single hole, they are elongated in the y -direction as was previously found by Waldman et al. [2003]. However, these authors further obtained that the piecewise-constant hoop stresses for two holes under shear-dominating loading are *exactly* the same as in the single hole case *independently* of the separation distance. In other words, the shear-loaded optimal shapes also fully eliminate the holes interaction like in the equistress case. In contrast, our stresses extrema $\max \sigma_{\theta\theta}(\theta) \approx 3.10$ and $\min \sigma_{\theta\theta}(\theta) \approx -2.85$ on Figure 8 are higher than the single-hole level $\sigma_{\theta\theta}(\theta) \approx 2.78843$ (the right-bottom cell of Table 2) and differ in their absolute values. The difference is too large to be attributed completely to numerical accuracy and, therefore, the above-mentioned conclusion is not entirely supported in the quantitative analysis.

5.4. Two V -optimal holes in a circular disk under uniform pressure ($\sigma_{nn} = P, \sigma_{n\tau} = 0$). As the last example, we consider a uniformly compressed disk with two identical traction-free side holes. Here, again, the symmetry relations (5-1) are obeyed, so that $\Phi(z)$ is written as

$$\Phi(z) = \sum_{k=1}^{\infty} d_{2k}^{(0)} z^{2k} + \sum_{k=1}^{\infty} d_k^{(1)} \left(\frac{1}{(z - a_1)^k} - \frac{(-1)^k}{(z + a_1)^k} \right), \tag{5-8}$$

$$z \in S + L, \quad a_1 \in S_1, \quad \text{Im } d_k^{(0,1)}, \quad k = 2, 3, \dots$$

In contrast to the equistress case (Section 5.1), the elastic domain is now finite and described by two dimensionless parameters, namely the relative area $f_{1,2} = f_{1,2}/\pi R^2 < 0.5$ of the hole and its displacement $x_0 < R$ from the center of the disk, where R is the disk radius.

Figure 10 depicts the identified V -optimal holes against their circular counterparts. Qualitatively, the resultant shape is rather predictable because at given $f_{1,2}$ and x_0 the V -optimization strives to move the hole away from the fixed outer boundary at the expense of the inner disk part. The corresponding

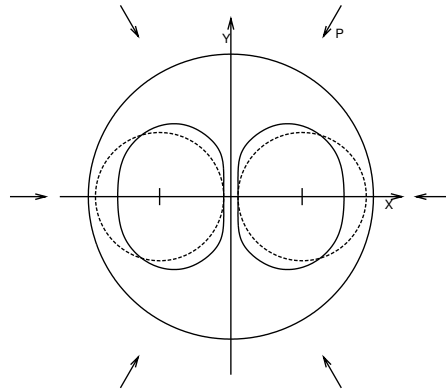


Figure 10. A uniformly compressed disk with two V -optimal holes at $x_0 = 0.05$ and $f_{1,2} = 0.2025$. The circular holes of the same location and area (dashed lines) are also shown for comparison.

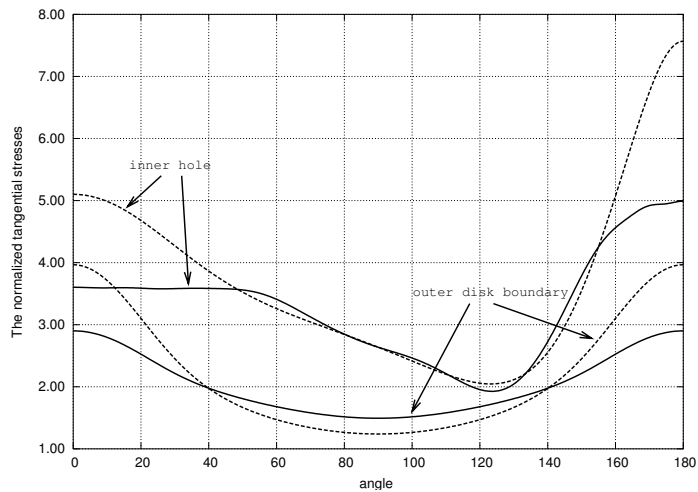


Figure 11. A uniformly compressed disk with two V -optimal holes at $x_0 = 0.05$ and $f_{1,2} = 0.2025$. The resultant tangential stress distributions (solid lines) versus their counterparts for circular holes (dashed lines).

stress distributions are shown in [Figure 11](#). As one might expect, the V -criterion not only smooths the hoop stresses but also drastically reduces them as compared to the standard circular holes. The observed deviations of the V -optimal distributions from the equistress value $\sigma_{\theta\theta} \equiv 2$ measure the influence of the disk's circular boundary.

6. Concluding remarks

A new optimality criterion of smoothing the hoop stresses along holes in a perforated two-dimensional elastic body has been proposed to extend the equistress principle (3-1) for the general case when neither the equi- nor M -equistress shapes exist. For efficient numerical simulations, the criterion was combined

with a complex variable-base direct solver and an economical shape encoding scheme as the main ingredients of an evolutionary optimization process, each especially tailored for the problem at hand. Of them, only the stresses variation criterion is really novel. Though related to the local stress distributions, it has an integral form thus offering substantial numerical advantages. Within the proposed simulation approach the V -criterion runs as a powerful filter of spurious oscillations of the hoop stresses thus permitting to effectively smooth and reduce them at moderate computational cost. It is worthy to note again that the V -optimal distribution tends to be piecewise constant what is absolutely a nontrivial solution. The results presented demonstrate the promise of applying it to shape optimization in other fields of continuum mechanics.

References

- [Abramowitz and Stegun 1964] M. Abramowitz and I. A. Stegun (editors), *Handbook of mathematical functions with formulas, graphs, and mathematical tables*, National Bureau of Standards Applied Mathematics Series **55**, U.S. Government Printing Office, Washington, DC, 1964.
- [Ahlfors 1978] L. V. Ahlfors, *Complex analysis: An introduction to the theory of analytic functions of one complex variable*, 3rd ed., McGraw-Hill, New York, 1978.
- [Banichuk 1977] N. V. Banichuk, “Optimality conditions in the problem of seeking the hole shapes in elastic bodies”, *Prikl. Matem. Mekhan.* **41**:5 (1977), 920–925. In Russian; translation in *J. Appl. Math. Mech.*, **41**:5, 946–951.
- [Cherepanov 1974] G. P. Cherepanov, “Inverse problems of the plane theory of elasticity”, *Prikl. Mat. Mekh.* **38**:6 (1974), 963–979. In Russian; translated in *J. Appl. Math. Mech.* **38**:6 (1974), 915–931.
- [Courant 1950] R. Courant, *Dirichlet’s principle, conformal mapping, and minimal surfaces*, Interscience, New York, 1950. Reprinted Dover, New York, 2005.
- [Goldberg and Sastry 2010] D. Goldberg and K. Sastry, *Genetic algorithms: the design of innovation*, Springer, New York, 2010.
- [Milton 2002] G. W. Milton, *The theory of composites*, Cambridge Monographs on Applied and Computational Mathematics **6**, Cambridge University Press, Cambridge, 2002.
- [Muskhelishvili 1963] N. I. Muskhelishvili, *Some basic problems of the mathematical theory of elasticity: fundamental equations, plane theory of elasticity, torsion and bending*, 2nd ed., Noordhoff, Leiden, 1963. Reprinted 1975.
- [Natanson 1955] I. P. Natanson, *Theory of functions of a real variable*, Frederick Ungar, New York, 1955.
- [Vigdergauz 1976] S. B. Vigdergauz, “Integral equation of the inverse problem of the plane theory of elasticity”, *Prikl. Mat. Mekh.* **40**:3 (1976), 566–569. In Russian; translated in *J. Appl. Math. Mech.* **40**:3 (1976), 518–522.
- [Vigdergauz 2006] S. B. Vigdergauz, “Energy-minimizing hole in an elastic plate under remote shear”, *J. Mech. Mater. Struct.* **1**:2 (2006), 387–406.
- [Vigdergauz 2008] S. B. Vigdergauz, “Shape optimization in an elastic plate under remote shear: from single to interacting holes”, *J. Mech. Mater. Struct.* **3**:7 (2008), 1341–1363.
- [Vigdergauz 2010] S. B. Vigdergauz, “Energy-minimizing openings around a fixed hole in an elastic plate”, *J. Mech. Mater. Struct.* **5**:4 (2010), 661–677.
- [Vigdergauz and Cherkaev 1986] S. B. Vigdergauz and A. V. Cherkaev, “A hole in a plate optimal for its biaxial extension-compression”, *Prikl. Mat. Mekh.* **50**:3 (1986), 524–528. In Russian; translated in *J. Appl. Math. Mech.* **50**:3 (1986), 401–404.
- [Waldman et al. 2003] W. Waldman, M. Heller, and L. F. Rose, “Shape optimisation of two closely spaced holes for fatigue life extension”, Report DSTO-RR-0253, Defence Science and Technology Organization, Australian Department of Defence, 2003, Available at <http://www.dsto.defence.gov.au/publications/2558/>.

Received 30 May 2010. Revised 11 Oct 2010. Accepted 13 Oct 2010.

SHMUEL VIGDERGAUZ: smuel@iec.co.il

Research and Development Division, The Israel Electric Corp. Ltd., P.O.Box 10, 31000 Haifa, Israel

JOURNAL OF MECHANICS OF MATERIALS AND STRUCTURES

<http://www.jomms.org>

Founded by Charles R. Steele and Marie-Louise Steele

EDITORS

CHARLES R. STEELE Stanford University, U.S.A.
DAVIDE BIGONI University of Trento, Italy
IWONA JASIUK University of Illinois at Urbana-Champaign, U.S.A.
YASUhide SHINDO Tohoku University, Japan

EDITORIAL BOARD

H. D. BUI École Polytechnique, France
J. P. CARTER University of Sydney, Australia
R. M. CHRISTENSEN Stanford University, U.S.A.
G. M. L. GLADWELL University of Waterloo, Canada
D. H. HODGES Georgia Institute of Technology, U.S.A.
J. HUTCHINSON Harvard University, U.S.A.
C. HWU National Cheng Kung University, R.O. China
B. L. KARIHALOO University of Wales, U.K.
Y. Y. KIM Seoul National University, Republic of Korea
Z. MROZ Academy of Science, Poland
D. PAMPLONA Universidade Católica do Rio de Janeiro, Brazil
M. B. RUBIN Technion, Haifa, Israel
A. N. SHUPIKOV Ukrainian Academy of Sciences, Ukraine
T. TARNAI University Budapest, Hungary
F. Y. M. WAN University of California, Irvine, U.S.A.
P. WRIGGERS Universität Hannover, Germany
W. YANG Tsinghua University, P.R. China
F. ZIEGLER Technische Universität Wien, Austria

PRODUCTION

PAULO NEY DE SOUZA Production Manager
SHEILA NEWBERY Senior Production Editor
SILVIO LEVY Scientific Editor

Cover design: Alex Scorpan


Cover photo: Ev Shafrir

See inside back cover or <http://www.jomms.org> for submission guidelines.

JoMMS (ISSN 1559-3959) is published in 10 issues a year. The subscription price for 2010 is US \$500/year for the electronic version, and \$660/year (+\$60 shipping outside the US) for print and electronic. Subscriptions, requests for back issues, and changes of address should be sent to Mathematical Sciences Publishers, Department of Mathematics, University of California, Berkeley, CA 94720-3840.

JoMMS peer-review and production is managed by EditFLOW™ from Mathematical Sciences Publishers.

PUBLISHED BY

 **mathematical sciences publishers**
<http://www.mathscipub.org>

A NON-PROFIT CORPORATION

Typeset in L^AT_EX

©Copyright 2010. Journal of Mechanics of Materials and Structures. All rights reserved.

A semianalytical solution for the bending of clamped laminated doubly curved or spherical panels	
KASRA BIGDELI and MOHAMMAD MOHAMMADI AGHDAM	855
Analytical solution for a concentrated force on the free surface of a coated material	
ZHIGEN WU, YIHUA LIU, CHUNXIAO ZHAN and MEIQIN WANG	875
On the nonlinear dynamics of oval cylindrical shells	
S. M. IBRAHIM, B. P. PATEL and Y. NATH	887
Time-harmonic elastodynamic Green's function for the half-plane modeled by a restricted inhomogeneity of quadratic type	
TSVIATKO V. RANGELOV and GEORGE D. MANOLIS	909
An enhanced asymptotic expansion for the stability of nonlinear elastic structures	
CLAUS DENCKER CHRISTENSEN and ESBEN BYSKOV	925
Stress and strain recovery for the in-plane deformation of an isotropic tapered strip-beam	
DEWEY H. HODGES, ANURAG RAJAGOPAL, JIMMY C. HO and WENBIN YU	963
Assessment of the performance of uniform monolithic plates subjected to impulsive loads	
JONAS DAHL	977
Stress smoothing holes in planar elastic domains	
SHMUEL VIGDERGAUZ	987
Numerical simulation of failed zone propagation process and anomalies related to the released energy during a compressive jog intersection	
XUE-BIN WANG, JIN MA and LI-QIANG LIU	1007